Numerical simulation of air inlet sound insulation

Julien Puig, Jean-François Deü, Walid Larbi, Mathieu Aucejo

inter·noise 2021
1–5 August | Washington, DC

Numerical simulation of air inlet sound insulation

Julien Puig[1], Jean-François Deü[2], Walid Larbi[3], Mathieu Aucejo[4]
Laboratoire de Mécanique des Structures et des Systèmes Couplés Conservatoire national des arts et Métiers - Le Cnam
292 rue Saint-Martin - 75003 Paris

ABSTRACT

Breathing healthy air at home requires an efficient ventilation which is generally achieved by mechanically controlled ventilation systems. However, the installation of air inlets, at the top of windows, reduces sound insulation. Nowadays, laboratory tests must be processed by manufacturers to measure the SRI (sound reduction index), which is calculated from the difference between the source and receiving sound power levels in the one-third octave band. The addition of melamine, a widely used porous material with interesting acoustic properties, slightly decreases the transmitted noise through air inlets, but the sound reduction remains far from that of a window without any inlet at all. Moreover, experimental settings induce uncertainties, particularly when low frequencies are involved. Numerical simulation is thus an interesting alternative for studying air inlets' vibro-acoustic behavior. Many parameters can be considered without the need to carry out new experiments, thus greatly reducing financial costs. Calculations must be computationally efficient to enable an optimization approach. To this end, the proposed model combines analytical and numerical solutions using the patch transfer function method which is a substructuring approach. Here, each subsystem of complex geometries is discretized by finite elements and porous materials are modelled using an equivalent fluid or localized impedance.

1. INTRODUCTION

To date, the sound insulation of air-inlets is measured by manufacturers in acoustic laboratories. As shown in Figure 1, the experimental conditions consist in a rigid-walled emitting room coupled to a rigid-walled receiving room, with an opening where the tested air-inlet is placed. The design of the emission room is supposed to guarantee a diffuse pressure field on the incident surface of the air-inlet, which is on the external part for real configurations. A loudspeaker emits a white noise, and the mean sound power level is measured on both rooms by a set of microphones. Such a configuration induces uncertainties on the measured SRI, which is the indicator used by manufacturers to define the acoustic performance of an air-inlet. Indeed, size of the rooms, mounting system, location of the loudspeaker and microphones can change the pressure field and the accuracy of the measurements,

[1]julien.puig@lecnam.net
[2]jean-francois.deu@cnam.fr
[3]walid.larbi@lecnam.net
[4]mathieu.aucejo@lecnam.net

making air-inlet testing hardly reproducible.

Hence, numerical modelling becomes an efficient way to improve acoustic efficiency of air-inlet. To date, there is no digital tool specifically dedicated to the calculation of the sound insulation of a complex air inlet which integrates porous materials. Some FEM and BEM based models have been developed to estimate the sound transmission of windows and openings in buildings [1, 2], with relatively simple geometries. The influence of absorbers on ventilation windows is investigated in [3]. In this article, a numerical model of air-inlet is presented. A diffuse pressure field is applied on the incident surface, the power transmitted is calculated with Rayleigh integral on the radiation surface, and porous materials are considered with equivalent fluid or localized impedance models. Then, a substructuring approach, the Patch Transfer Function method [4], is considered to take the influence of the rooms into account, combining analytical and finite element calculations.

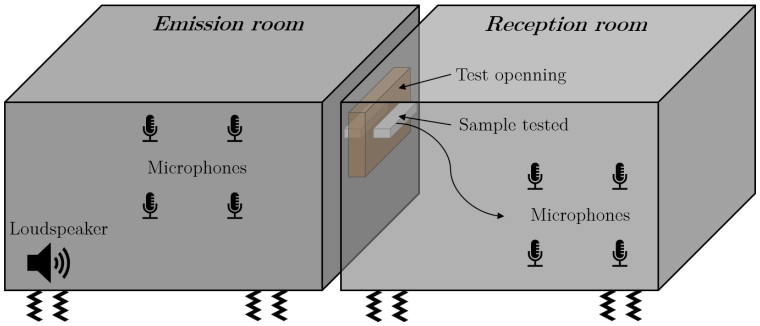

Figure 1: Measurement of air-inlet sound insulation

2. AIR-INLET SOUND REDUCTION INDEX

In building acoustics, the sound reduction index is the indicator generally used to quantify the sound insulation of walls, windows, or specific materials. It is calculated as follows:

$$R = L_1 - L_2 + 10\log\left(\frac{S}{A}\right) \tag{1}$$

with L_1 the mean sound power level in the emission room, L_2 the mean sound power level in the reception room, S the sample area and A the equivalent absorbing area of the reception room calculated with Sabine formula [5]. However, this indicator is unsuitable for air-inlets because they do not have a well-defined sample area and the acoustic insulation is not necessarily proportional to their dimensions. Therefore, Dn,e is preferred by manufacturers to quantify the acoustic absorption of air-inlet, it is defined as:

$$D\text{n,e} = L_1 - L_2 + 10\log_{10}\left(\frac{A_0}{A}\right) \tag{2}$$

with A_0 a reference area fixed at 10m^2. Experimental measures of Dn,e are averaged on one-third octave band. A unique value is often used to quantify the general acoustic performance of air-inlets : the Dn,e,w, which is calculated from the Dn,e according to standard ISO717 [6].

On the other hand, the numerical model which is presented in section 3 computes a classical transmission loss (TL), which describes the intrinsic acoustic performance of air-inlets:

$$TL = 10\log_{10}\left(\frac{P_{\text{rad}}}{P_{\text{inc}}}\right) \tag{3}$$

where P_{rad} is the transmitted acoustic power at the air-inlet radiation surface and P_{inc} the acoustic power applied on the air-inlet incident surface. So, the TL calculated by the model does not take the rooms into account and will be compared to the Dn,e measured in laboratory, averaged in one-third octave band.

Regardless of the sample tested, experimental measurements of Dn,e have frequently a peak at low frequency (<250 Hz), corresponding to a wavelength larger than 1.4 meter, which is far greater than the characteristic dimension of air-inlet (40 cm). For these frequencies, the pressure field is almost uniform in the air-inlet, thus the transmission losses should only depend on the opening surface and should be nearly constant. Therefore, we can already suppose that the room has a non-negligible influence on the measurements.

3. INTRINSIC ACOUSTIC BEHAVIOR OF THE AIR-INLET

This section presents the details of the numerical model used to compute the intrinsic air-inlet transmission loss. Comparisons are made between Dn,e measured in acoustic laboratory and TL computed by the model.

3.1. Incident and radiated acoustic power

A diffuse pressure field is applied on the incident surface of the air-inlet. This exciting field is obtained as a sum of N decorrelated incident plane waves of angles θ_n and ϕ_n and random phases ψ_n (see Figure 2):

$$p_0(x,y) = \frac{1}{\sqrt{N}} \sum_{n=1}^{N} e^{-i\left(k_{n,x}x + k_{n,y}y\right)} e^{i\psi_n} \tag{4}$$

where:

$$\begin{aligned} k_{n,x} &= k_0 \sin\theta_n \cos\phi_n \\ k_{n,y} &= k_0 \sin\theta_n \sin\phi_n \end{aligned} \tag{5}$$

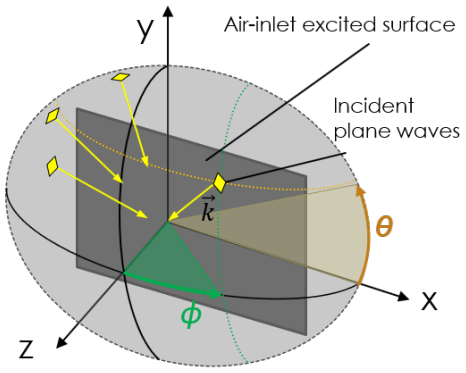

Figure 2: Generation of diffuse pressure field on the incident surface

The incident acoustic power can be deducted from this applied pressure field:

$$P_{inc} = \frac{1}{2} \int_S Re\left(p_0 v_0^*\right) dS \approx \frac{S}{4\rho_0 c_0} \bar{p}_0^2 \tag{6}$$

with $\bar{p}_0^2$ the mean quadratic value of the incident pressure, ρ_0 the density, c_0 the speed of sound, S the area of the incident surface and v_0 the normal velocity.

The radiated power is obtained from the normal velocity on the radiation surface (located in the receiving room). It can be calculated by discretizing the radiation surface into a set of R elementary radiators as explained in [7]. The radiation resistance matrix $[R]$ is defined:

$$[R] = \frac{\omega^2 \rho_0 A_e^2}{4\pi c_0} \begin{bmatrix} 1 & \frac{\sin(kR_{12})}{kR_{12}} & \dots & \frac{\sin(kR_{1R})}{kR_{1R}} \\ \frac{\sin(kR_{21})}{kR_{21}} & 1 & \dots & \dots \\ \dots & \dots & \dots & \dots \\ \frac{\sin(kR_{R1})}{kR_{R1}} & \dots & \dots & 1 \end{bmatrix} \tag{7}$$

with ω the pulsation, R_{ij} the distance between elementary radiators i and j and A_e the surface of the elementary radiators. Then, the radiated power is calculated using the radiation resistance matrix and the normal velocity vector $\{\tilde{v}_e\}$:

$$P_{\text{rad}} = \{\tilde{v}_e\}^H [R] \{\tilde{v}_e\} \tag{8}$$

3.2. Finite element model of air-inlet

The acoustic problem is presented in Figure 3. A transmission loss is calculated in the fluid domain Ω_f between the incident surface Γ_{inc} and the radiation surface Γ_{rad}. A rigid wall boundary condition is applied on Γ. Porous material volumes Ω_p have been considered as equivalent fluid and Johnson-Champoux-Allard (JCA) model was used [8,9]. It is also possible to consider only the porous interface Γ_p, applying a localized complex impedance Z_p on it to reduce computing costs [10]. A diffuse pressure field p_0 is applied on the incident surface (see equation 4) and the pressure at the radiation surface is set to 0.

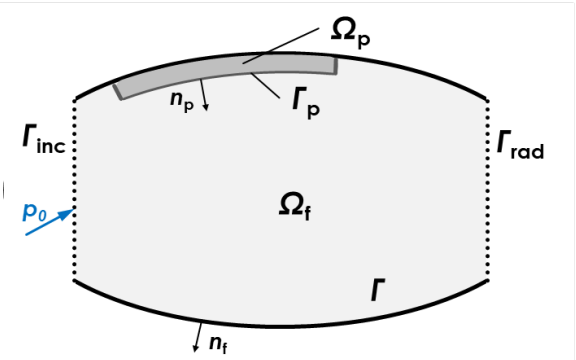

Figure 3: Definition of the acoustic problem

The acoustic problem is governed by the following equations:

$$\begin{cases} \Delta p(\mathbf{x},\omega) + k_0^2 p(\mathbf{x},\omega) & \forall \mathbf{x} \in \Omega_\text{f} \\ p(\mathbf{x},\omega) = p_0(\mathbf{x},\omega) & \forall \mathbf{x} \in \Gamma_{\text{inc}} \\ \dfrac{\partial p}{\partial \mathbf{n_f}}(\mathbf{x},\omega) = \mathbf{0} & \forall \mathbf{x} \in \Gamma \\ p(\mathbf{x},\omega) = 0 & \forall \mathbf{x} \in \Gamma_{\text{rad}} \\ + \text{ porous material equations (see below)} \end{cases} \tag{9}$$

with k_0 the acoustic wave number.

The equation related to the behavior of the porous material depends on the model used. If JCA model is chosen, we have:

$$\Delta p\left(\mathbf{x},\omega\right)+k_{\mathrm{eq}}^{2}p\left(\mathbf{x},\omega\right)\qquad\forall\mathbf{x}\in\Omega_{\mathrm{p}}\tag{10}$$

where the acoustic wave number k_{eq} is given by JCA formulation [9]. Otherwise, the impedance condition on Γ_{p} is defined as follow:

$$\frac{1}{\rho}\nabla p.\mathbf{n}_{\mathrm{p}}=-p\frac{i\omega}{Z_{\mathrm{p}}}\qquad\forall\mathbf{x}\in\Gamma_{\mathrm{p}}\tag{11}$$

where Z_{p} is calculated from acoustic parameters as explained in [10].

All numerical calculations are based on the finite element method. The geometry of real samples has been reproduced with CAD software, before being meshed. All the physical domains are meshed in 3D with 10 nodes quadratic tetrahedral elements.

3.3. Comparison with experimental measurements

The sample tested is showed in Figure 4. The parameters of the porous material used (melamine) are described in Table 1.

Table 1: Acoustic parameters of melamine. (E, ν, η, ρ) relate to the solid phase (Young's modulus, Poisson ratio, mechanical loss factor, density) and (σ, ϕ, α_∞, Λ, Λ') relate to the fluid phase (resistivity, porosity, tortuosity, viscous and thermal lengths).

	E	ν	η	ρ	σ	ϕ	α_∞	Λ	Λ'
Units	Pa	-	-	kg.m^{-3}	Pa.s/m^2	-	-	μm	μm
Melamine	10^5	0.4	0.05	9.0	15 300	0.96	1.02	105	205

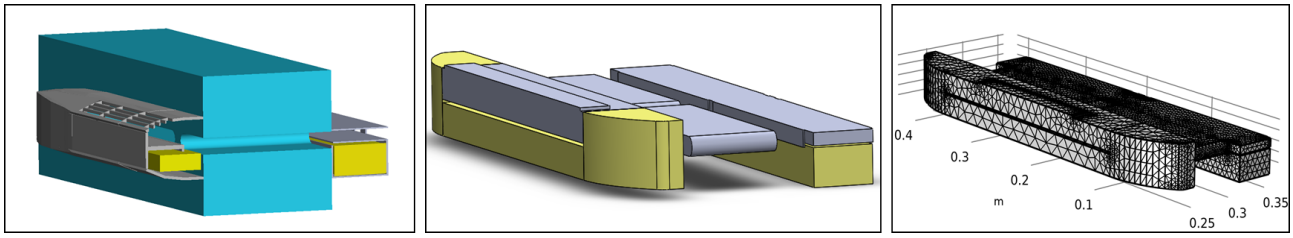

Figure 4: Sample tested. Left: cut view of the air-inlet CAD model; Center: simplification and extraction of the physical volumes (air in grey and melamine in yellow); Right: finite element mesh.

This sample is the most complete configuration which was tested, with all parts of an air-inlet. Comparison of numerical and experimental results is showed on Figure 5. It appears that the curves do not fit well. Nevertheless, some conclusions can be considered. First, the increasing of transmission loss when melamine foam is added is visible in the experimental measures as well as in the simulation results. Secondly, in all cases, the simulations give a transmission loss almost constant for the frequency below 500 Hz. As explained before, the fact that air-inlet is small compared to the wavelength for theses frequencies can explained the phenomenon. Finally, the overall shape

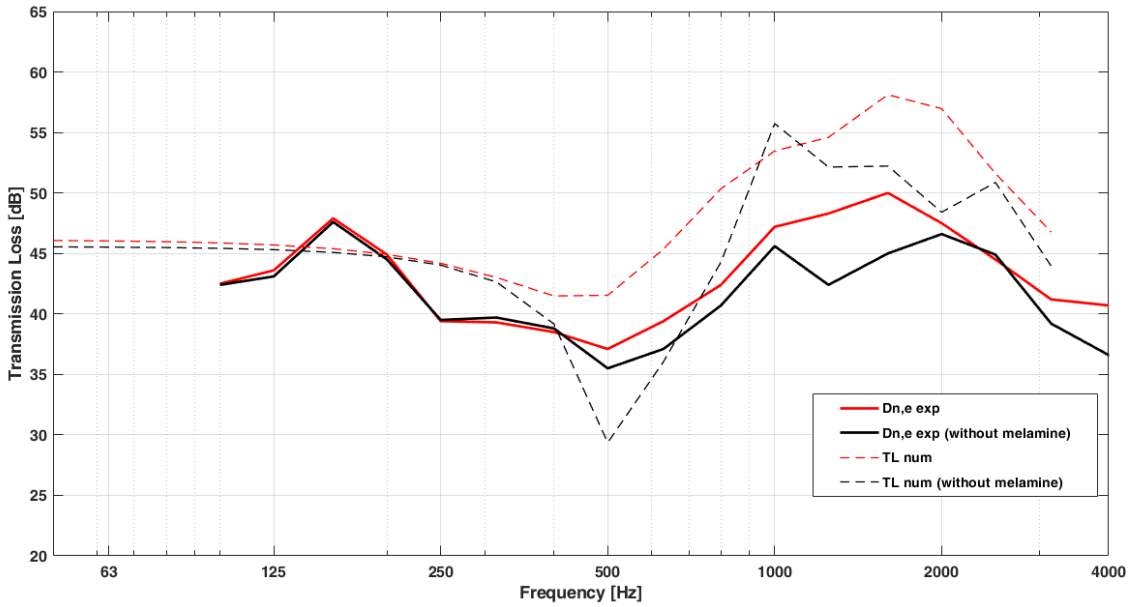

Figure 5: Comparison between experimental and numerical results. Solid line: experimental measures, dash: simulation

of the curves for the sample with melamine is similar, the gap is approximately constant with the frequency. This gap could has several sources: the fixations of the air-inlet, the internal geometry which is slightly different (real sample including various small parts), the influence of the rooms, the parameters of melamine used or even the indicators used (as previously said, the TL considers only the air-inlet while the Dn,e depends on the rooms).

These elements drive to the conclusion that rooms cannot be neglected for air-inlet sound transmission studies. Obviously, because of their sizes, computation of the rooms using finite elements would induce prohibitive calculation costs. Then, it becomes necessary to consider a sub-structuring approach for reducing calculation time, and later enable an optimization approach. In this work, we have chosen to use the PTF method whose principle and first application are presented in the following section.

4. PATCH TRANSFER FUNCTION METHOD

Patch transfer function method is a substructuring approach for studying complex acoustic problems. It consists in the discretization in several patches of the coupling surface between two sub-systems [4, 11, 12]. The transfer functions of each uncoupled system are calculated on the patches and are assembled using continuity equations on the interface (pressure and velocity). Then, the pressure field of the coupled system can be rebuilt. The equations of the method are briefly presented and applied over two geometries. Firstly, a rectangular rigid box cut in two parts is considered, analytical and numerical results are compared. Then, a more representative system composed of three subdomains - two rooms coupled with a parallelepiped air-inlet - is considered.

4.1. Description of the method

The patch transfer method is explained with a simple example: a 3D rectangular rigid acoustic domain (Figure 6). Considering a monopole source S vibrating at the pulsation ω, placed in the domain Ω, the pressure on the listening point L can be analytically calculated as an infinite sum of

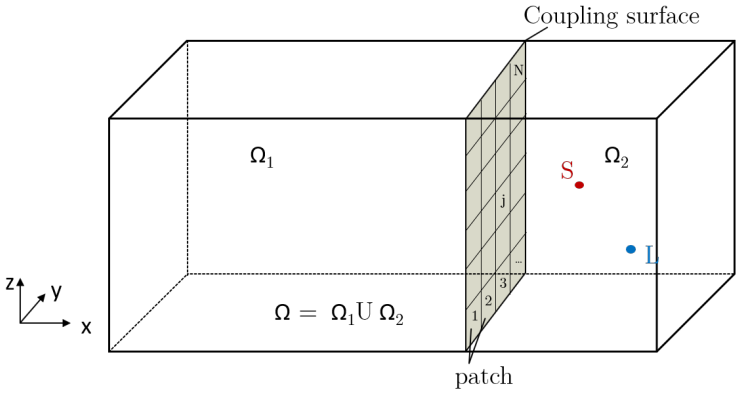

Figure 6: Coupled system and subdomain definition

modal contributions:

$$P(L,S,\omega) = Q(\omega)\, c^2 \sum_{k=1}^{\infty} \frac{\phi_k(L)\,\phi_k(S)}{\left(\omega^2 - \omega_k^2 - i\eta_k\omega_k\omega\right)\Lambda_k} \tag{12}$$

where Q is the acoustic source debit, c is the speed of sound, ϕ_k, ω_k, η_k, and Λ_k are respectively the modal shape, the pulsation, the modal damping and the norm of mode k. This solution will be later compared with PTF calculation.

Considering that the domain Ω is an assembly of the subdomain Ω_1 and Ω_2, the contribution of each sub-domain has to be calculated on the coupling surface, divided into N patches. Mathematically, a patch transfer function is an impedance averaged on a patch surface. For the acoustic cavity c, we define the PTF Z^c_{jk} between an excited patch k and a receiver patch j, as the ratio of the averaged pressure $\bar{p}^c_j$ on the patch j and the averaged normal velocity $\bar{v}^c_k$ on the patch k:

$$Z^c_{jk} = \frac{\bar{p}^c_j}{\bar{v}^c_k} \tag{13}$$

where $\bar{\blacksquare}_p = \dfrac{1}{S_p}\int_{S_p} \blacksquare dS$ is the space average on the patch p of surface S_p.

Likewise, on the acoustic cavity c, the PTF Z^c_{jL} is the ratio of the averaged pressure $\bar{p}^c_j$ on the patch j and the normal velocity $v^c(L)$ on the point L:

$$Z^c_{jL} = \frac{\bar{p}^c_j}{v^c(L)} \tag{14}$$

With these definitions, the space averaged pressure $\bar{p}^c_j$ on the patch j on each uncoupled system is exclusively related to the velocity $\bar{v}^c_k$ of all patches k and potential source term $\bar{\tilde{p}}^c_j$ (in the example, the source is in Ω_2). The pressure can be expressed as following:

$$\bar{p}^c_j = \bar{\tilde{p}}^c_j + Z^c_{jk}\bar{v}^c_k \tag{15}$$

The coupling of the subdomains Ω_1 and Ω_2 is based on the continuity of pressure and velocity on each patch of the coupling surface. For a patch j, coupling conditions are:

$$\begin{cases} \bar{p}^{\Omega_1}_j = \bar{p}^{\Omega_2}_j = \bar{p}_j \\ \bar{v}^{\Omega_1}_j = -\bar{v}^{\Omega_2}_j = \bar{v}_j \end{cases} \tag{16}$$

This yields to the following matrix system with unknown vector $\left\{\bar{v}_j\right\}$:

$$\begin{cases} \left\{\bar{p}_j^{\Omega_1}\right\} = \left[Z_{jk}^{\Omega_1}\right]\left\{\bar{v}_j\right\} \\ \left\{\bar{p}_j^{\Omega_2}\right\} = \left[Z_{jk}^{\Omega_2}\right]\left\{\bar{v}_j\right\} + \left\{\tilde{\bar{p}}_j^{\Omega_2}\right\} \end{cases} \tag{17}$$

Finally, the pressure p(L) at the listening point L is the sum of patches contribution (equation 14) and eventual source contribution (equation 12). With $\tilde{p}_L^{\Omega_2}$ the pressure at the listening point generated by the source (in this case: the source and the listening point are in the same subdomain), we have:

$$p\,(L) = \left[Z_{jL}^{\Omega_2}\right]\left\{\bar{v}_j\right\} + \tilde{p}_L^{\Omega_2} \tag{18}$$

The PTF approach is well suited for studying complex geometries as each subsystem is solved independently, with its own model. Particularly, PTF matrices of each subsystem can be calculated analytically (all analytical PTF for the rigid box are given in [12]) or numerically. Thus, the update of one of the subsystems only requires the update of the PTF of this subsystem, provided that the coupling surface remains the same. Furthermore, when PTF are computed with finite element method, the use of incompatible mesh at the coupling surface is possible as the quantities evaluated are averaged on the patches. Two applications of the PTF are presented in the next section.

4.2. Application on simple geometries

The geometry used for the presentation of PTF method was firstly tested to validate the implementation on MATLAB. The parameters are taken from [12] and stated in Table 2. Three calculations are compared: the analytical solution in the whole cavity Ω, the PTF method with only analytical results for calculation of PTF matrices and the PTF method where the impedance matrix of cavity Ω_1 is computed numerically while the matrix of cavity Ω_2 is computed analytically. Two patches are chosen and results are shown on Figure 7. The curves match together and are the same as the ones obtained by Grialou [12].

Table 2: Geometrical and physical parameters of the system presented on Figure 6. All lengths are in meters.

	Ω	Ω_1	Ω_2
$(L_x\,;\,L_y\,;\,L_z)$	(0.8 ; 0.4 ; 0.2)	(0.5 ; 0.4 ; 0.2)	(0.3 ; 0.4 ; 0.2)
Source S	(0.75 ; 0.06 ; 0.07)	-	(0.25 ; 0.06 ; 0.07)
Listening point L	(0.72 ; 0.28 ; 0.15)	-	(0.22 ; 0.28 ; 0.15)
ρ	1.29 kg.m^{-3}		
c	340 m.s^{-1}		
η	0.02		
$(L_x\,;\,L_y)$ Patches	2 patches of size (0.20 ; 0.20)		

Then, a larger model was considered, with no analytical solution. As the goal is to show that PTF method can be used for studying acoustic of air-inlets, the geometry chosen (Figure 8) is made of three rigid boxes with two coupling surfaces. Then, this configuration is similar to the emission-sample-reception one, presented in Figure 1, in terms of subdomains considered. The subdomains Ω_1 and Ω_3 refer respectively to an emission and a reception room (even if the boxes presented are smaller in order to keep a fully numerical calculation possible) and the subdomain Ω_2

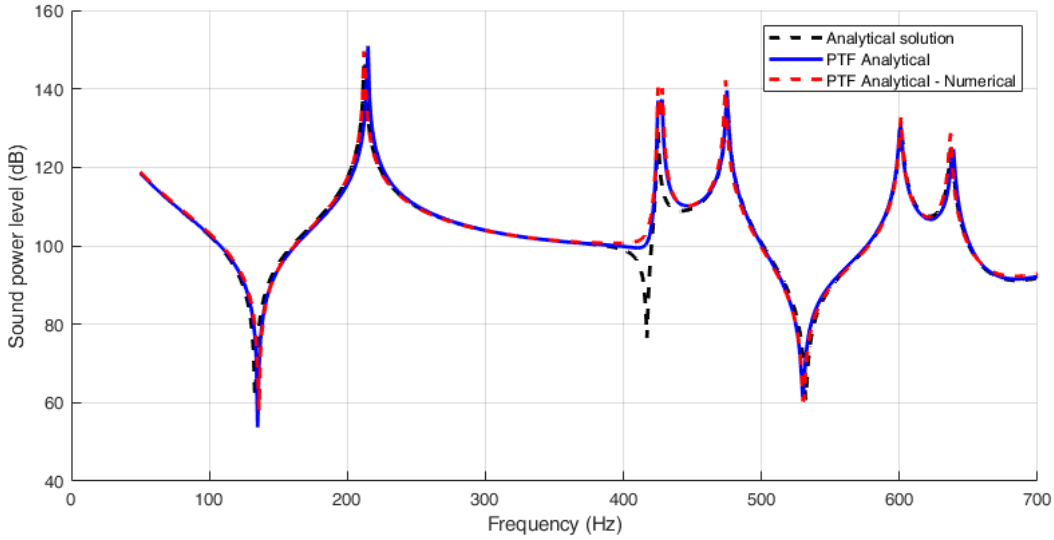

Figure 7: Comparison between the analytical solution (equation 12), the PTF method with both subdomains computed analytically and the PTF method with Ω_1 computed numerically and Ω_2 computed with finite elements.

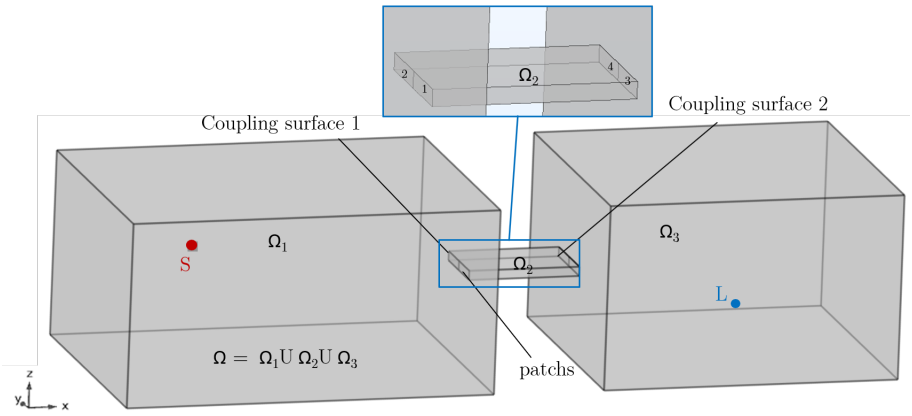

Figure 8: Definition of the complex geometry studied with a PTF approach.

represents a simplified air-inlet.

In this configuration, the first coupling surface has N_1 patches and the second has N_2 patches. A subscript is added to the variables (pressure and velocity) to specify the coupling surface concerned. The equations are written on each subdomain, the unknown is the average normal velocity of the patches $\left\{\bar{v}_j\right\}_{1,2}$:

$$\begin{cases} \left\{\bar{p}_j^{\Omega_1}\right\}_1 = \left[Z_{jk}^{\Omega_1}\right]\left\{\bar{v}_j\right\}_1 + \left\{\bar{p0}_j^{\Omega_2}\right\}_1 \\ \left\{\bar{p}_j^{\Omega_2}\right\}_{1,2} = \left[Z_{jk}^{\Omega_2}\right]\left\{\bar{v}_j\right\}_{1,2} \\ \left\{\bar{p}_j^{\Omega_3}\right\}_2 = \left[Z_{jk}^{\Omega_3}\right]\left\{\bar{v}_j\right\}_2 \end{cases} \tag{19}$$

Here, matrices $\left[Z_{jk}^{\Omega_1}\right]$, $\left[Z_{jk}^{\Omega_2}\right]$ and $\left[Z_{jk}^{\Omega_3}\right]$ are respectively $N_1 \times N_1$, $(N_1 + N_2) \times (N_1 + N_2)$ and $N_2 \times N_2$.

With the continuity of pressure and velocity, the solution of the system 19 is the following:

$$\left\{\bar{v}_j\right\}_{1,2} = \left(\begin{bmatrix}\left[Z_{jk}^{\Omega_1}\right] & 0_{N_1\times N_2}\\ 0_{N_2\times N_1} & \left[Z_{jk}^{\Omega_3}\right]\end{bmatrix} + \left[Z_{jk}^{\Omega_2}\right]\right)^{-1} \begin{Bmatrix}\left\{\bar{p}_j^{\Omega_1}\right\}_1\\ 0_{N_2\times N_1}\end{Bmatrix} \tag{20}$$

Finally, the pressure $P(L)$ can be computed:

$$P(L) = \left[Z_{jL}^{\Omega_3}\right]\left\{\bar{v}_j\right\}_2 \tag{21}$$

The dimensions of each subdomains are stated in Table 3. Firstly, fully numerical calculation were made to evaluate the pressure $P(L)$ at the listening point. Frequencies are taken from 50 to 1000 Hz with a 2 Hz step. The convergence of the mesh has been obtained with a $\lambda/7$ criterion. Then, a semi-analytical PTF configuration is considered with only the subdomain Ω_2 computed numerically and both Ω_1 and Ω_3 computed analytically. Two patches were chosen for both coupling surfaces ($N_1 = N_2 = 2$). The last configuration is fully analytical. All the configuration are showed on the Figure 9. The full model took almost 21 hours to complete while the PTF model lasted about 10 minutes. The results displayed on Figure 10 show a perfect match of the two PTF model, and a good match with the numerical calculation.

Table 3: Geometrical and physical parameters of the system presented on Figure 8. All lengths are in meters.

	Ω_1	Ω_2	Ω_3
(x ; y ; z)	(0 ; 0 ; 0)	(2.0 ; 0.55 ; 0.475)	(2.6 ; 0 ; 0)
(L_x ; L_y ; L_z)	(2.0 ; 1.5 ; 1)	(0.6 ; 0.4 ; 0.05)	(1.6 ; 1.5 ; 1.0)
Source S	(0.5 ; 0.6 ; 0.7)		
Listening point L	(3.5 ; 0.4 ; 0.3)		
ρ	1.29 kg.m^{-3}		
c	340 m.s^{-1}		
η	0.02		
(L_x ; L_y) Patches	2 patches of size (0.20 ; 0.05)		

Convergence of the PTF method can be analysed in a future work using in particular the solution based on an analytical modelling of each subdomain.

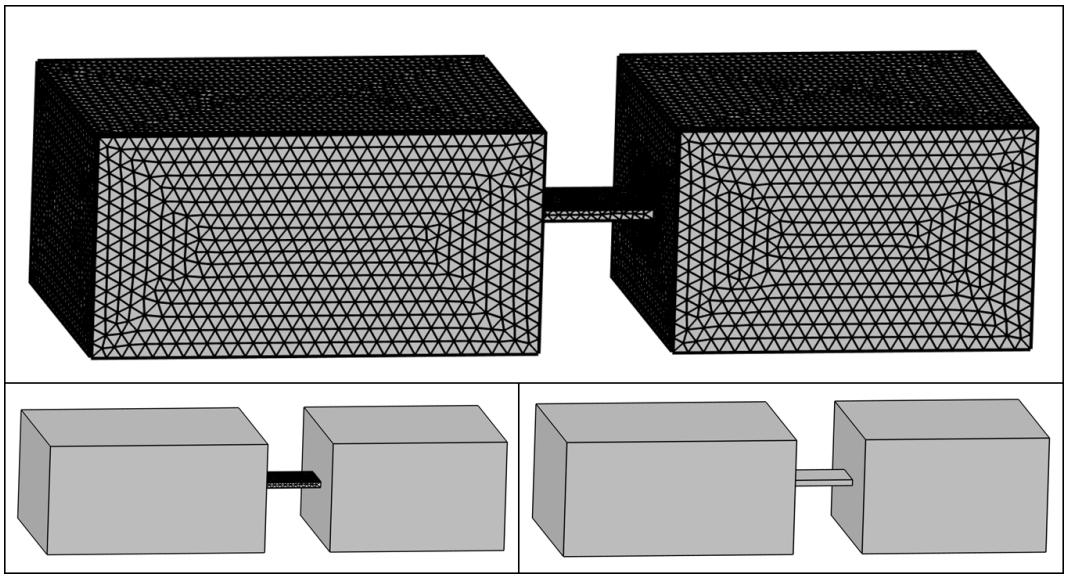

Figure 9: 3 configurations are compared. At the top: the full mesh of the numerical calculation (1 074 662 dofs). At the bottom left: the mesh (2 965 dofs) used with semi-analytical PTF method. At the bottom right: a view of the full geometry calculated with fully analytical PTF method.

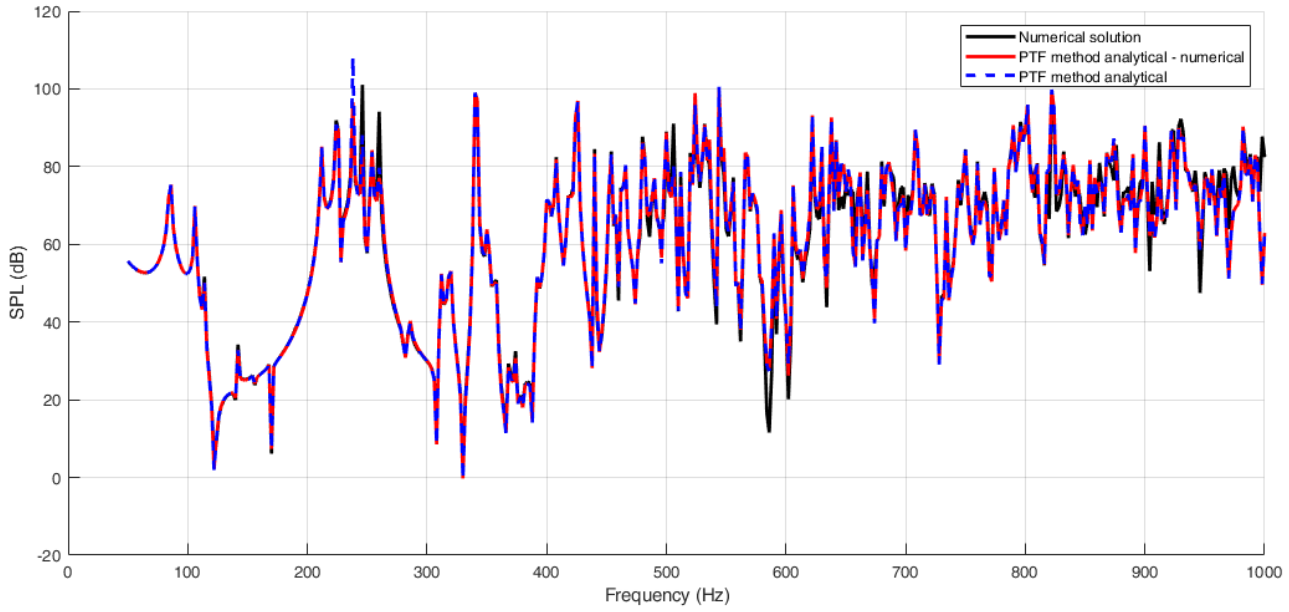

Figure 10: Comparison of the sound power level at the listening point calculated with the full FE model, the semi-analytical PTF method and the fully analytical PTF method. 2 patches were chosen.

5. CONCLUSIONS

Differences have been highlighted between experimental Dn,e and TL computed by the intrinsic air-inlet model. These differences are supposed to result from the influence of the emission and reception rooms on measurements. Therefore, a configuration constituted by a simple geometry linked with rooms is investigated using PTF method. This sub-structuration approach appears to be an efficient way to consider the emission and reception rooms without increasing sharply calculation time, thus enabling optimization procedures. The next step will be to use this method on air-inlets to investigate the room influence. It will be necessary to define an interface that does not change while substituting the measured sample. Uncertainties were not considered so far, but upcoming developments will present a way to combine PTF method and uncertainties.

ACKNOWLEDGEMENTS

The authors would like to express their thanks to CODIFAB (Comité professionel de développement des industries françaises de l'ameublement et du bois) for its financial support.

References

[1] P. Jean. Modeling of sound transmission through air inlets. 16th International Congress on Sound and Vibration, 2009.

[2] C. Soussi, M. Aucejo, W. Larbi, and J.-F. Deü. Numerical analyses of the sound transmission at low frequencies of a calibrated insulating glazing unit. *Applied Acoustics*, 179:108065, 2021.

[3] X. Yu, S.-K. Lau, L. Cheng, and F. Cui. A numerical investigation on the sound insulation of ventilation windows. *Applied Acoustics*, 117:113–121, 2017.

[4] M. Ouisse, L. Maxit, C. Cacciolati, and J.-L. Guyader. Patch transfer functions as a tool to couple linear acoustic problems. *Journal of Vibration and Acoustics*, 127:458–466, 2005.

[5] *NF EN ISO 10140 : Acoustique - Mesurage en laboratoire de l'isolation acoustique des éléments de construction*, 2013.

[6] *NF EN ISO 717 : Acoustique - Évaluation de l'isolement acoustique des immeubles et des éléments de construction*, 2013.

[7] F. Fahy and P. Gardonio. *Sound and Structural Vibration*. Elsevier, 2nd edition, 2007.

[8] D. Johnson, J. Koplik, and R. Dashen. Theory of dynamic permeability and tortuosity in fluid-saturated porous media. *Journal of Fluid Mechanics*, 176:379–402, 1987.

[9] Y. Champoux and J.-F. Allard. Dynamic tortuoisty and bulk modulus in air-saturated porous media. *Journal of Applied Physics*, 70:1975–1979, 1991.

[10] Q. Serra, M. Ichchou, and J.-F. Deü. On the use of transfer approaches to predict the vibroacoustic response of poroelastic media. *Journal of Computational Acoustics*, 176:1550020, 2016.

[11] L. Maxit, M. Aucejo, and J.-L. Guyader. Modelling of sound transmission through ship structures using the patch transfer functions approach. 40th International Congress and Exposition on Noise Control Engineering, 2011.

[12] M. Grialou. *Vibro-acoustics substructuring : Combining simulations and experimental identification of subdomains for low frequency vehicle acoustics*. PhD thesis, INSA de Lyon, 2018.